

**A numerical study of the cloud microphysical properties in the East China Sea region
by a bin-type cloud resolving model**

東シナ海領域を対象としたビン法雲解像モデルによる雲微物理特性に関する数値実験

Takamichi Iguchi

Doctoral Dissertation

Department of Earth and Planetary Science Graduate School of Science

The University of Tokyo

February 28, 2006

Abstract

A system of regional cloud resolving models have been developed by combining a three-dimensional non-hydrostatic dynamic model and particle microphysical models that can treat cloud, aerosol and radiation processes to simulate cloud and aerosol stratifications in an area around the East China Sea. Simulations were performed with a nesting algorithm applied to the distribution of aerosol concentration, which is given from a global simulation of an aerosol transport model coupled with a general circulation model, for reproducing the horizontal and vertical distributions of tropospheric aerosols and/or cloud condensation nuclei in this area. The models can compute characteristic parameters that reflect the size distributions of hydrometeors represented in the particle microphysical model. These simulated parameters have been compared from those obtained by remote sensing observations with latest satellite sensors.

It was found that obtained simulation results well reflect the general feature of the aerosol and cloud distributions observed by Terra/MODIS remote sensing of aerosol and cloud microphysics and Radar-AMeDAS precipitation analysis. Problems in the simulation were a systematic bias in the simulated effective particle radius of water clouds and an overestimation of the total frequency of 1-hr precipitation amount. The particle radius bias was reduced by an adjustment of input cloud condensation nuclei (CCN) concentration based on the comparison with data by aircraft measurements. This result indicates that the CCN concentration affects the cloud microphysical properties and must be given suitably to bring the simulation result to comparable values to the satellite-observed values. On the other hand, the adjusted CCN concentration did not reduce the overestimation in the frequency of accumulated precipitation. The CCN sensitivity test indicated that the CCN amount did not significantly affect the precipitation amount in our cases, where a synoptic-scale forcing such as baroclinic instability was dominant to determine the development of clouds. That was due to a compensation of two competing processes, i.e., a reduction in the precipitation efficiency and an increase in the cloud liquid water amount due to increased CCN amount.

A bulk-type cloud scheme can be used to reproduce accurate distribution of the precipitation amount in the short-term simulation for cases in which a background forcing in synoptic-scale is dominant and/or the cloud microphysical properties is not important to determine the development of the field, as in the situation of the weather forecast with enough initialization by observed fields. A bin-type cloud scheme, on the other hand, seems to be more useful for a short-term simulation for specific cases, in which there is no background forcing, and a longer-term simulation than a bulk-type scheme. An accurate cloud microphysical property calculated by the bin-model has potentiality to improve the effect of the cloud field to slowly responding processes, such as radiative heating and cooling,

SST change and so on.

Acknowledgements

The study in this doctor thesis is based on helpful supports by many people. Firstly, I am grateful to Prof. T. Nakajima of the Center of Climate System Research (CCSR), the University of Tokyo for many advises and encouragements to the whole of my study. I would like to thank former senior students in the laboratory, Prof. T. Takemura of the Research Institute for Applied Mechanics, Kyushu University for the offer of aerosol simulated results by the SPRINTARS with CCSR/NIES-AGCM and special advises about aerosol, Dr. K. Suzuki of the CCSR, the University of Tokyo for the offer of data about global scale CCN sensitivity and special support about cloud microphysics, and Prof. M. Sekiguchi of the Department of Marine Electronics and Mechanical Engineering, Tokyo University of Marine Science and Technology for the offer of a radiation code, mstrn-x and special advises about radiation.

I wish to acknowledge Dr. K. Saito and other developers of the Japan Meteorological Agency Numerical Prediction Division and the Meteorological Research Institute for the development of JMA-NHM and MRI/NPD-NHM, and also acknowledge Prof. A. P. Khain and other developers of the Hebrew University Cloud Model for its development.

I acknowledge Prof. T. Y. Nakajima of the Tokai University for the production and offer of Terra/MODIS cloud retrieval data and RGB Images, Dr. A. Higurashi of the National Institute for Environmental Studies for the offer of Terra/MODIS aerosol retrieval data, and Prof. Y. Ishizaka of the Nagoya University for the offer of CCN and cloud datasets by the aircraft measurement. I would also like to thank all the staff concerning the Asian Atmospheric Particulate Environment Change Studies project.

The numerical simulations in this study are made, using the computational servers of the CCSR and the massive computational server, SR 11000, of the Information Technology Center, the University of Tokyo.

Contents

Chapter 1	General Introduction	7
1.1	Effect of aerosol on cloud	7
1.2	Objectives of this study	9
Chapter 2	Regional cloud resolving modeling	11
2.1	Introduction	11
2.2	Model development	12
2.2.1	Introduction	12
2.2.2	Main dynamics framework	13
2.2.3	Cloud microphysical modeling	14
2.2.4	Aerosol microphysical modeling	15
2.2.5	Radiation process modeling	16
2.2.6	Integration of the dynamical and microphysical models	17
2.3	Setup of numerical experiments	19
2.4	Observation data compared with simulated results	20
2.5	General weather condition of the targeted days	21
	Appendix 2A: The basic dynamics equations	23
	Appendix 2B: Bin-type cloud microphysical scheme	24
	Appendix 2C: CCN in the bin-type cloud microphysical scheme based on HUCM	27
	Appendix 2D: Code parallelization and calculation cost	29
Chapter 3	Aerosol distribution simulated by a nesting method	32
3.1	Introduction	32
3.2	Comparison with the result of SPRINTARS	33
3.3	Comparison with satellite data	34
3.4	Conclusions	38
Chapter 4	Simulation of cloud microphysical property and its relation with CCN	39
4.1	Introduction	39
4.2	Model validation with satellite cloud retrieval data and aircraft CCN measurements	40
4.2.1	Case on 13 March 2005	40
4.2.2	Case on 8 April 2003	41
4.2.3	Case on 2 April 2003	44
4.3	Conclusions	49
Chapter 5	Simulation of precipitation and its relation with CCN	50
5.1	Introduction	50
5.2	Comparison with Radar-AMeDAS precipitation analysis	50
5.3	Sensitivity test for CCN concentration	51

5.4 Conclusions.....	55
Chapter 6 Discussions.....	56
6.1 Significance of introducing bin-type cloud microphysical model.....	56
6.2 Supplementary numerical experiments.....	56
6.3 Discussion with a prior study for the similar nest-grid simulations	60
6.4 Comparison with global scale study about CCN sensitivity.....	61
Chapter 7 General conclusions	63
References.....	71

Chapter 1 General Introduction

1.1 Effect of aerosol on cloud

A cloud is a colloidal suspension system of water and/or ice particles. The cloud droplets are formed in the process of water vapor condensation around hydrophilic aerosols in the atmosphere. These aerosols are called cloud condensation nuclei (CCN). There are characteristic differences in the cloud properties in each environment that has different CCN concentration and characteristics. A well-known example of this phenomenon is the systematic difference between cloud properties over continents and over ocean, where aerosol concentrations are largely different [e.g., *Squires*, 1956]. Observations showed that maritime cumulus had a smaller concentration of droplets than that found in continental cumulus. Mean radii of droplets in maritime cumulus were typically larger than those in continental cumulus. These systematic differences of cloud microphysical properties result from a positive correlation between concentrations of CCN and droplets.

Once CCN change the cloud microphysical properties, the radiative budget of the atmosphere also changes through a perturbed radiative property of the cloud system. By this mechanism, anthropogenic air pollution can cause a large influence on the cloud characteristics and the radiative budget of the earth. This is called the aerosol indirect effect. *Twomey* [1974] pointed out that an increase in the aerosol concentration produces an increase in the cloud droplet concentration, assuming that the cloud liquid water path does not change. Then he concluded that the albedo of an optically thin cloud increases by an increase in the aerosol concentration, whereas the albedo of an optically thick cloud such as a deep convective cumulus decreases when aerosols include light absorbing substances. The latter phenomenon is caused by the enhanced absorption of solar radiation through cloud multiple scattering. Because thin clouds with optical thickness less than 20 are dominant in the earth's atmosphere, an increase in anthropogenic aerosols that work as CCN may cause a global cooling. On the other hand, *Albrecht* [1989] found that an increase in the cloud droplet concentration prevents the growth of droplets by the coagulation process and suppresses the generation of large droplets such as drizzle and rain droplets. This effect extends the cloud lifetime so that the liquid water path and/or fraction of clouds increase to produce a further global cooling.

To quantify the magnitude of the climate change caused by the aerosol indirect effect, extensive studies have been performed for evaluating the radiative forcing by anthropogenic aerosols on a global scale. *Charlson et al.* [1992] estimated that the radiative forcing of the aerosol indirect effect due to only sulfate aerosols is -1 W/m^2 if the anthropogenic aerosol concentration is assumed to increase by 15% after the industrial revolution. *Hansen et al.* [1998] calculated the radiative forcing values for three types of aerosols (i.e., sulfate, organic

carbon, and soil dust). *Nakajima et al.* [2001] estimated that the radiative forcing is in a range of $-0.7 \sim -1.7 \text{ W/m}^2$, assuming that the aerosol concentration had increased by 15 % ~ 40 %, from an analysis of satellite remote-sensing data.

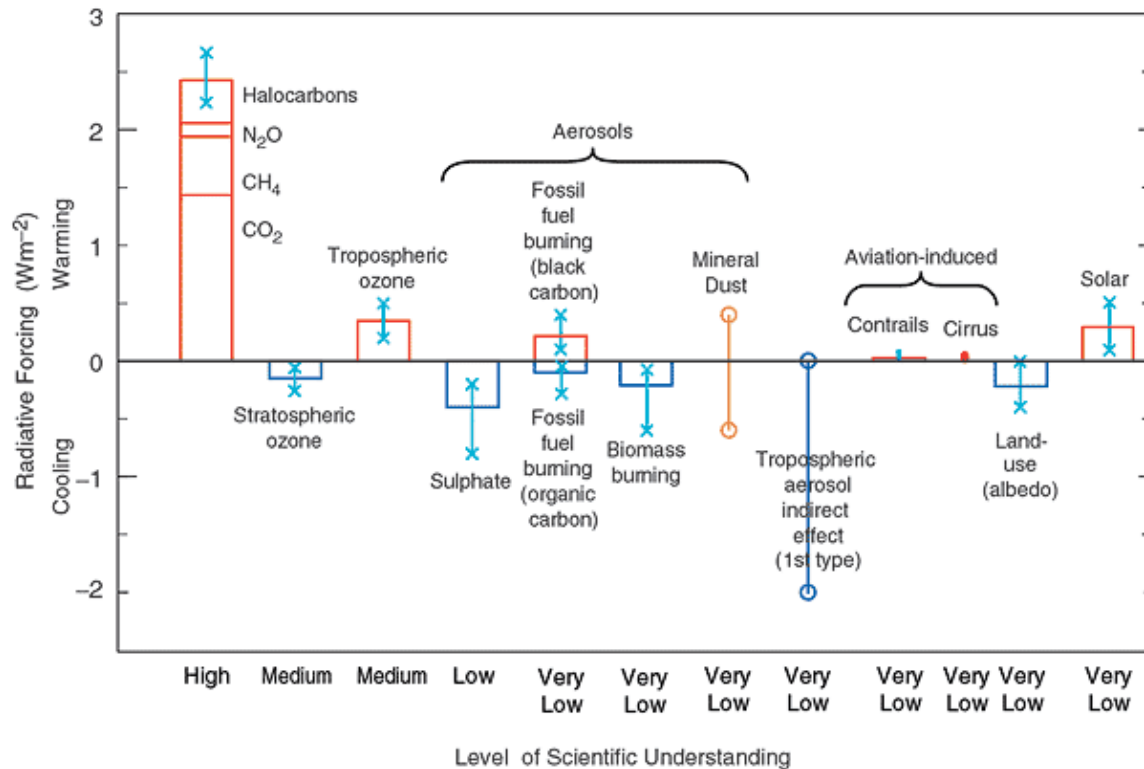


Figure 1.1 Estimation of the annual and global mean radiative forcing of the climate system for the year 2000 relative to 1750, from the *Intergovernmental Panel on Climate Change* [2001].

The general circulation model (GCM) simulation has been used for investigating global distributions of observables regarding the cloud properties, like cloud optical thickness and effective particle radius, and for evaluating the radiative forcing of aerosol indirect effects. However, a realistic aerosol and cloud interaction cannot be accurately simulated by GCMs, because the cloud lifetime is too short and the cloud distribution is temporally and spatially too complicated to be treated by simplified parameterizations used in GCMs. The simulation results of the aerosol indirect effect by GCMs are thus highly dependent on the parameterization. *Pan et al.* [1998] investigated the uncertainty included in the estimation method of the radiative forcing by the aerosol indirect effect due to anthropogenic sulfate aerosols in GCMs. In their study the uncertainty was analyzed for five different GCMs with twenty input parameters using a probabilistic collocation method [*Tatang et al.*, 1997]. They concluded that the uncertainty of the radiative forcing by the indirect effect depends on the

difference in input parameter values than on the model structure. *Suzuki et al.* [2004] showed that the GCM-simulated correlation slope between cloud microphysical parameters and the aerosol concentration largely varies depending on adopted auto-conversion parameterizations. As a result, various GCM estimates of the radiative forcing of anthropogenic aerosols range from 0 to -2.5 Wm^{-2} at the top of the atmosphere [e.g., *IPCC*, 2001] (Fig. 1.1).

1.2 Objectives of this study

Under this situation, model simulations by high-resolution models, which can represent aerosol and cloud processes more directly, are important for studying the effects of aerosols (CCN) on clouds. In this dissertation, we developed a regional cloud resolving models, which are based on a Numerical Weather Prediction (NWP) model combined with a detailed cloud microphysical model suitable for cloud resolving simulations. In order to reproduce the real atmospheric condition, we adopted a nesting algorithm with a pre-calculated field of the outer model or re-analysis data, so that the simulated results are verified against observation directly. A notable advantage of the developed models is to introduce a nesting algorithm not only with a dynamical field but with a field of aerosols concentration, so that the models can set the initial and lateral boundary condition of aerosols to represent their realistic distribution in the nest-grid simulation.

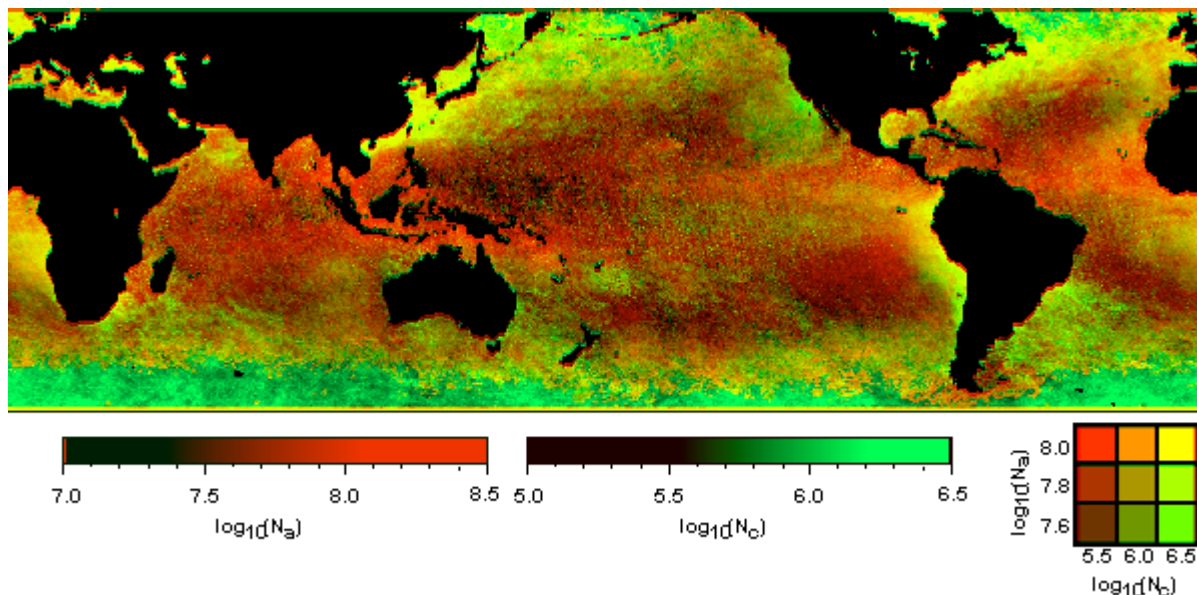


Figure 1.2 Global distribution of the correlation between column aerosol number (N_a) and column cloud particle number (N_c) (particles/ cm^2) as a four month average of 1990, obtained by analysis of channels of AVHRR [*Nakajima et al.*, 2001, Figure 3].

The numerical model under development has to meet the following two demands: to represent accurately realistic 4-d distribution of aerosols and to reproduce cloud microphysics affected by aerosols. Then, the following goals have to be achieved with the model: to verify a performance of the model by a comparison between simulated results and observation data; to investigate the sensitivity of the cloud and precipitation systems to the CCN concentration; to discuss future prospects of the models.

A region trimmed around the East China Sea is selected as a domain for which numerical simulations are carried out. Figure 1.2 shows the global distribution of the column aerosol number and the column cloud particle number as a four month average of 1990, which is obtained by AVHRR analysis. The yellow color means that concentrations of aerosols and cloud particles are high, so that there is strong interaction between them in these regions. A strong interaction between aerosols and cloud particles in the East China Sea region has been observed as in Fig. 1.2. In this region, there are also useful observational datasets acquired by the Asian Atmospheric Particulate Environment Change Studies (APEX) conducted as a Core Research Project for the Evolutional Science and Technology of Japan Science and Technology Agency (CREST/JST) [Nakajima *et al.*, 2003].

A description of the model development is given in chapter 2; aerosol distribution representation with a nesting algorithm is shown in chapter 3; chapters 4 and 5 present simulation results of cloud microphysical properties and precipitation, and then their correlation relation with CCN concentration; discussion and a summary are presented in chapters 6 and 7.

Chapter 2 Regional cloud resolving modeling

2.1 Introduction

In this chapter, a description of the regional cloud resolving model developed in this study is presented. There are two mathematical representations that are generally used in high-resolucional models to represent the particles size distribution in the cloud microphysics. One is a bulk (moment) method that predicts variables such as cloud mixing ratio and number concentration represented by integrated values of a prescribed size-distribution function. Another is a bin (spectral) method in which the size-distribution functions of cloud hydrometeors are approximated by a number of discrete size bins and are predicted by a cloud microphysics scheme. Significant quantities for simulation are changes in the cloud droplet number concentration, mean radius, and total volume, which cause a change in the radiation property and residence time of clouds. Therefore, the bin method, which is able to directly estimate the particle size spectra, is more suitable than a bulk method to study the aerosol indirect effects. Cloud microphysical variables such as the effective particle radius, which is one of the important observables from satellite remote sensing, can be estimated directly by integrating the binned size-distribution function.

Many high-resolution models have been developed to include a bin-type cloud microphysical scheme. *Arnason and Greenfield* [1972], for example, simulated cloud droplet nucleation from sea salt particles and condensation/evaporation processes in a two-dimensional grid model. *Kogan* [1991] developed a three-dimensional non-hydrostatic anelastic model for the warm rain microphysical processes that includes nucleation, condensation, evaporation, coalescence, breakup, and sedimentation. The simulation showed the evolution of a multi-cellular cloud and the change of droplet size distribution function. *Chen and Lamb* [1994] simulated cloud microphysical and chemical processes with a hybrid bin method, which conserves two moments (number and mass) of hydrometeors. *Khain et al.* [1999] simulated a convective cloud with mixed-phase cloud microphysical processes, using a 2-D version of Hebrew University Cloud Model (HUCM). They confirmed that an increase in the aerosol particle concentration leads to a decrease in the rate of warm rain formation and increase in the ice crystal formation. *Feingold and Kreidenweis* [2002] included an aqueous chemistry process and applied a bin method to the aerosol system with the aid of a large eddy simulation model. *Takahashi and Shimura* [2004] investigated the tropical rain characteristics and microphysics by five different microphysical model settings for a mixed-phase cloud simulation with a three-dimensional cloud model.

In most of the past studies using a bin-type microphysical model, however, simulations were performed under a simple condition such as in the assumption of a horizontally uniform boundary condition with an idealized convection and/or a large eddy simulation. The

advantage of such simple simulations is to realize accurate dynamical and microphysical calculations for a single cloud or clusters under a high calculation cost of the bin method. However, the result of such simulations depends on the assumption of boundary conditions and large-scale disturbances. Besides, the result is difficult to be compared with observational data, which is needed for validation of the model itself.

Thus, a new bin-type cloud resolving model, which can reproduce the complex condition corresponding to the real atmosphere, is needed to be developed. In this regard, NWP models fit to our demands. *Lynn et al.* [2005a, 2005b] is one of studies with such model. They developed a fast version of bin-type microphysical model based on a microphysical package contained within HUCM and implemented it into the nonhydrostatic mesoscale modeling system, the fifth-generation Pennsylvania State University–National Center for Atmospheric Research (Penn State–NCAR) Mesoscale Model (MM5) [e.g. *Dudhia*, 1993; *Grell et al.*, 1994]. Then, they presented simulated results of cloud systems over Florida on 27 July 1991 and compared the results to those from a version of the bulk-type cloud microphysical scheme.

In this study, a system of several versions of regional cloud resolving models has been developed by combining a NWP model and physical process schemes for cloud, aerosol, and radiation processes including a bin-type cloud microphysical scheme. Each version in the series has its own combination of the specialized schemes. This system, therefore, makes it possible to select a different versions depending on the purpose of the simulation. Then, comparisons among the results simulated with different versions provide more information to understand each process involved in the cloud formation phenomenon.

A detailed description of the model development is explained in section 2.2 and appendixes in this chapter; setup of the numerical experiments such as resolution is given in section 2.3; comparison of simulated results with observation data is introduced in section 2.4; section 2.5 explains the general weather condition of days targeted in the experiments.

2.2 Model development

2.2.1 Introduction

Numerical dynamics models used in this study are the operational model Non-Hydrostatic Model developed by the Numerical Prediction Division (NPD) of the Japan Meteorological Agency (JMA) in partnership with the Meteorological Research Institute (MRI) (JMA-NHM) [*Saito et al.*, 2006] and the outdated version, a multi-purpose Non-Hydrostatic atmospheric Model developed by the MRI and NPD of JMA (MRI/NPD-NHM) [*Saito and Kato*, 1999; *Saito et al.*, 2001]. JMA-NHM adopts an explicit three-ice bulk-type microphysical scheme [*Ikawa and Saito*, 1991; *Yamada*, 2003]. A bin-type cloud microphysical scheme has been

newly reconstructed in this study from the Hebrew University Cloud Model [Khain and Sednev, 1995, 1996; Khain *et al.*, 2000] to replace the bulk-type cloud scheme in the NHMs. We hereafter refer to this model framework as NHM+HUCM.

In order to make the NHM+HUCM interact with aerosols, we have developed a bin-type aerosol model by extending the model of Asanuma [2004] which was combined with a cloud resolving model [Suzuki *et al.*, 2006] for ideal simulations. The model has been extended to treat the five species of aerosols as same as aerosol species used in a Spectral Radiation Transport Model for Aerosol Species (SPRINTARS) [Takemura *et al.*, 2000, 2001] and to include several additional processes for a real-time simulation.

Miura *et al.* [2006] introduced a broadband radiative transfer code “mstrn-x” [Nakajima *et al.*, 2000; Sekiguchi and Nakajima, 2005], which was implemented in the CCSR/NIES-AGCM, into JMA-NHM replacing the JMA radiation code. We have modified the mstrn-x radiation code so as to accept bin-type size distribution functions of aerosol and cloud polydispersions generated by JMA-NHM+HUCM. We hereafter refer to this full bin-type aerosol and cloud model as CCSR/JMA/HU Bin-type Aerosol and Cloud Model (BACM).

Sub-section 2.2.2 presents descriptions of JMA-NHM and MRI/NPD-NHM which are the main frameworks of the JMA-NHM+HUCM; sub-sections 2.2.3, 2.2.4 and 2.2.5 explain BACM schemes for cloud, aerosol and radiation processes, respectively. In this way four versions of model have been developed by combination of the two dynamics frameworks (JMA-NHM and MRI/NPD-NHM) and the microphysical schemes for cloud, aerosol, and radiation processes, as described in sub-section 2.2.6.

2.2.2 Main dynamics framework

JMA-NHM has been the operational model of JMA since 1 September 2004. NHM are used for weather forecast to support disaster prevention and the very short range forecast of precipitation. 15-hr forecast is executed 8 times a day. The horizontal resolution in forecast operation is 5km and the domain size is 3,600 km x 2,880 km covering Japan and the surrounding region, projected on a map of Lambert coordinates. The main specifications of the model are listed in Saito *et al.* [2006, Table 1].

MRI/NPD-NHM is the outdated version of JMA-NHM. The model is a multi-purpose mesoscale model, which was developed by the MRI and NPD-JMA for both research and operational forecasting. Several modifications were added to improve its computational efficiency and precision.

The present model uses almost all computational routines of JMA-NHM and MRI/NPD-NHM such as dynamics, except for some physical processes. Non-hydrostatic fully compressible equations are used as the governing basic equations in NHMs. The basic

dynamics equations are summarized in appendix 2A. The NHMs have prepared two schemes to prevent the inflation of sound waves by restricting the maximum time-step: one is a scheme that treats waves implicitly in horizontal and implicitly in vertical (HI-VI scheme) and another is a scheme that treats waves explicitly in horizontal and implicitly in vertical (HE-VI scheme). In this study, we adopt the HI-VI scheme in the framework of MRI/NPD-NHM and the HE-VI scheme in the framework of JMA-NHM. The HI-VI scheme has a smaller calculation cost than the HE-VI scheme, but is unsuitable for a massive parallel computation in which the spatial grids are divided on plural nodes because the Helmholtz equation for pressure has to be solved. The Arakawa C type and the Lorentz type are used as the horizontal and vertical grid structure, respectively.

As for physical processes, cloud microphysics, aerosol microphysics, and radiation processes modeling are described in the latter sub-sections. Surface boundary layer process is calculated with Monin and Obukhov's similarity law. A four-layer ground model is used to calculate ground temperature. 1.5-order turbulent closure model, which is to calculate turbulent kinetic energy, is adopted to compute the diffusion coefficients. Fourth-order linear dumper is used to prevent from the development of computational noise.

2.2.3 Cloud microphysical modeling

An explicit three bulk-ice type microphysical scheme [*Ikawa and Saito, 1991; Yamada, 2003*] is originally equipped in JMA-NHM. In this scheme, hydrometeors are categorized into five species (cloud water, rain, cloud ice, snow, and graupel). Their mixing ratios are the prognostic variables in the model. For categorized rain, snow and graupel, inverse exponential functions are assumed for their size distribution functions. For cloud water and ice particles, mono-dispersive distribution is assumed and their gravitational falling is neglected. The cloud microphysical processes are illustrated in *Saito et al.* [2006, Figure 5 and Table 3]. The conversion process from cloud water into rain is parameterized with “Kessler’s parameterization” [e.g., *Kessler, 1969*] and the auto-conversion threshold value of 0.1 g Kg^{-1} .

A bin-type cloud microphysical scheme has been reconstructed in this study for JMA-NHM from the cloud microphysical module package within HUCM model [*Khain and Sednev, 1995, 1996; Khain et al., 2000*]. The scheme treats seven hydrometeors, i.e. water droplets, ice crystals (plate, column, dendrite), snowflakes, graupels, and hails. The size distribution functions of hydrometeors are discretized into 33 size bins by uniformly dividing the logarithm of the particle mass. For example, bins of water droplets roughly cover the radius range $2.0 \mu\text{m} < r < 325.1 \mu\text{m}$. The nucleation from CCN to droplets, nucleation to ice crystals, diffusion growth, evaporation, sublimation, droplet freezing, melting, and coagulation growth are represented by formulae as summarized in Appendix 2B. The

terminal velocities of hydrometeors for each size bin of hydrometeors are determined at the first time step, depending on the mass, types of hydrometeors, and the air density, and then the gravitational sedimentation of hydrometeors is calculated with a box-lagrangian scheme [Kato, 1995] to avoid the CFL condition.

In the original JMA-NHM, the Kain-Fritsch (K-F) convective parameterization scheme [e.g. Kain and Fritsch, 1993] was introduced as one of sub-grid convective parameterizations which can be selected in the model. However, a commonly accepted sub-grid convection parameterization suitable for a bin method have not been developed yet, so that no sub-grid convective parameterizations is used in the present numerical experiments in the main discourse.

2.2.4 Aerosol microphysical modeling

In the original HUCM model, a size distribution function of CCN is one of prognostic variables and their advection, diffusion and activation (nucleation to water droplets) are calculated. In our NHM+HUCM model, the same treatment of CCN is succeeded in the bin-type cloud microphysical scheme. The conservation equation of the size distribution function and the formula of activation process are summarized in Appendix 2C. The size distribution function of CCN consists of 33 size (mass) bins and the maximum CCN mass is set equal to the minimum mass of a drop in the drop spectrum (the minimum radius of the drop is 2 μm) in the original HUCM [Khain and Sednev, 1996], whereas our NHM+HUCM adopts the number of size bins as 13 with a radius range of binned CCN from about 1 μm to 10^{-3} μm .

In the original study of Khain and Sednev [1996] an initial field of CCN is assumed as the concentration decreases exponentially with height and is uniform horizontally. At the lateral boundaries, zero horizontal gradients of the CCN distribution are assumed. Other studies with bin-type cloud microphysical schemes adopt similar initialization and lateral boundary condition of the CCN concentration [e.g., Kogan, 1991; Lynn *et al.*, 2005a, 2005b].

Different from these past studies, we set an inhomogeneous initial field and a lateral boundary condition by introducing a nesting algorithm. The present model can be nested in a large domain, using interpolation of the field given by an outer model or analysis data in the same way as in the original JMA-NHM and MRI/NPD-NHM. The same nesting method is applied to the distribution of aerosol concentration given from global numerical simulation by SPRINTARS coupled with Center for Climate System Research / National Institute for Environmental Studies - Atmospheric General Circulation Model (CCSR/NIES-AGCM) [Numaguti, 1995] with a horizontal resolution of T106 and 20 vertical layers for five tropospheric aerosols (organic carbonaceous, black carbonaceous, soil dust, sulfate and sea salt). Among these aerosols, organic carbonaceous, sulfate and sea salt aerosols are assumed

to be hygroscopic and serve as CCN. A method of converting the concentrations of the hygroscopic aerosols to the size distribution function of CCN at each bin is summarized in Appendix 2C.

Table 2.1 Maximum and minimum edge radii and mode radii in each aerosol bin.

Aerosol type	minimum radii (μm)	mode radii (μm)	maximum radii (μm)
black carbonaceous	0.00236	0.118	5.9
soil dust	0.08	4	200
sea salt	0.04	2	100
sulfate sodium	0.00139	0.0695	3.475
organic carbonaceous	0.002	0.1	5

Our full bin-type aerosol and cloud model (CCSR/JMA/HU-BACM) adopts a bin-type aerosol model developed by *Asanuma* [2004], which was combined with a cloud resolving model [*Suzuki et al.*, 2006]. This model represented several processes, i.e. activation to droplets, gravitational settling, moisture absorption growth, and impaction scavenging of aerosols. We have extended this bin-type aerosol model to treat five tropospheric aerosols, two species of gases (dimethylsulfide (DMS) and SO_2), and SO_4^{2-} ions and to include several additional aerosol-related processes for a realistic simulation (emission from sea and land surface, dry deposition, gravitational settling, chemical reaction of sulfate species, re-emission from evaporated droplets, and accumulation), based on the corresponding algorithms implemented in SPRINTARS [*Takemura et al.*, 2000, 2001]. The organic carbonaceous, sea salt, and sulfate aerosols are hygroscopic particles that can be activated to droplets and grow by moisture absorption, whereas the black carbon and dust aerosols are assumed to be hydrophobic. The size distributions of these aerosols are represented with a bin method. The size distribution functions of aerosols are discretized into 7 size-bins by uniformly dividing the logarithm of the particle mass. The maximum and minimum edge radii of aerosols' bins are set as 50 times and 0.02 times as large as the typical mode radii. The radii are listed in Table 2.1. Inhomogeneous initial fields and lateral boundary conditions for five tropospheric aerosols and two species of gases are prepared by introducing the nesting method with SPRINTARS global simulation to drive this bin-type aerosol model.

2.2.5 Radiation process modeling

In the original JMA-NHM, the atmospheric radiation scheme is based on *Sugi et al.* [1990], which was implemented to MRI/NPD-NHM. Two schemes for treating an effect of

cloud can be selected from the original scheme by *Sugi et al.* [1990] and a scheme introduced by *Yamamoto and Satomura* [1994]. As for treatment of clouds, the former scheme adopts a cloud fraction parameterized as a function of relative humidity calculated for calculating long and short wave radiative fluxes. In the latter scheme liquid water path (LWP) and ice water path (IWP) are explicitly calculated from the mixing ratios of hydrometeors, and are used to calculate the radiative properties of clouds. In this study, we use the former radiation scheme in the framework of MRI/NPD-NHM.

A broadband radiative transfer code “mstrn-x”, which was developed in CCSR [*Nakajima et al.*, 1990; *Sekiguchi and Nakajima*, 2005] for radiation process calculation in the CCSR/NIES-AGCM. This code uses a k-distribution approximation and two stream delta-Gaussian scheme to calculate radiative fluxes taking into account the line and continuum absorption/emission, and multiple scattering by atmospheric molecules (H_2O , CO_2 , O_3 , N_2O , CH_4 , and O_2) and aerosol and cloud particles.

The radiative transfer calculation is performed at k-distribution channels in 18 wavelength bands in the whole spectral region from 0.2 μm to 200 μm . As for particulate matter, optical parameters (i.e. the extinction and absorption coefficients and moments of volume scattering function), which depend on radii and optical characteristics of the particulate matter, are prepared to compute the optical thickness and single scattering albedo of aerosols and clouds.

Mstrn-X was implemented in JMA-NHM by *Miura et al.* [2006]. We extended this version of mstrn-X to accept to both three bulk-ice type microphysical scheme and bin-type cloud microphysical scheme of NHM+HUCM and CCSR/JMA/HU CABM. In the case of the bin-type cloud scheme, the mode radius of hydrometeor is variable and calculated explicitly, so that the optical parameters are calculated depending on the species and mode radius of each hydrometeor. The “mstrn-x” code originally equipped with to CCSR/NIES-AGCM can treat gaseous absorption by CFCs and Halocarbons and radiation processes by aerosols, whereas the computation of these processes is omitted in the “mstrn-x” module built in JMA-NHM.

2.2.6 Integration of the dynamical and microphysical models

Four versions of the regional cloud resolving model are developed in this dissertation, by integrating different dynamical and microphysical models among the models introduced in the former sub-sections (Fig. 2.1). Each of them can be performed as an individual model. They have different performance about cloud, aerosol, and radiation processes, so that we can select the best version according to the objectives of simulation.

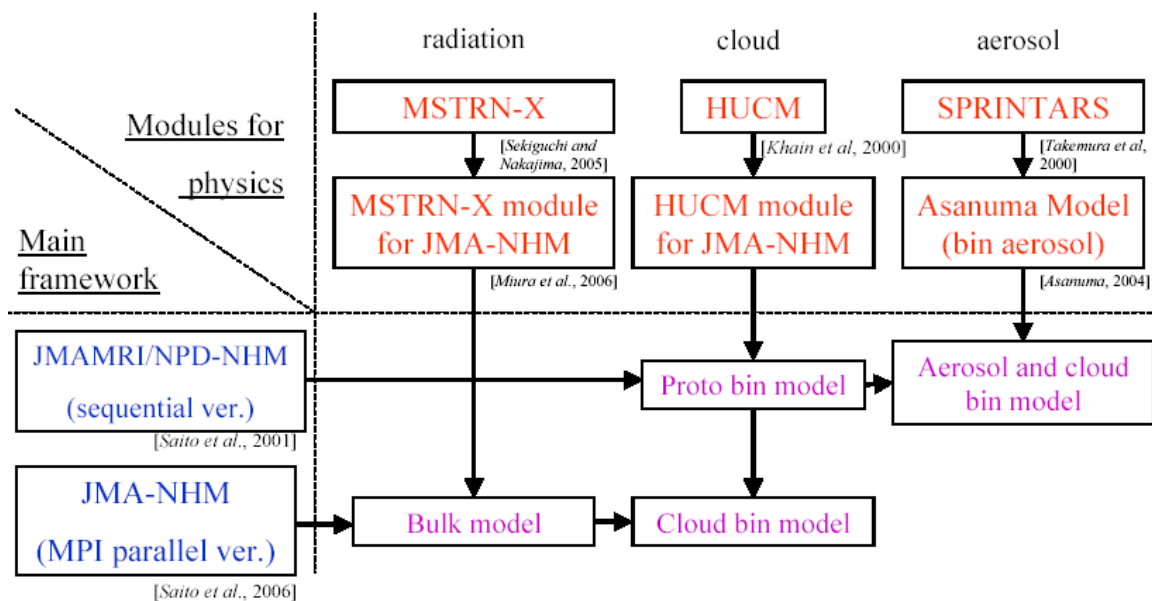


Figure 2.1 Flow chart showing the development of versions of regional cloud resolving model.

One of the four versions is “Proto bin model” consisting of MRI/NPD-NHM and the bin-type cloud scheme instead of the original bulk-type cloud scheme (Fig. 2.1). This version can treat water and ice cloud processes, i.e. nucleation from CCN to droplets, diffusion growth, evaporation, and coagulation growth, in a computational run of a three-dimensional simulation.

The “Aerosol and cloud bin model” version consists of MRI/NPD-NHM and bin-type aerosol and cloud scheme. The size ranges for aerosols and hydrometers are abstracted in Fig. 2.2. The bin-type aerosol and cloud scheme is introduced only into this version in the four versions. . This version can treat only water cloud processes in a run for a three-dimensional simulation for the same reason as the “Proto bin model” version.

The “Bulk model” version is essentially same as JMA-NHM, other than the radiation code replaced by “mstrn-x”. This version can treat water and ice cloud microphysical processes described for the original bulk-type cloud scheme, which does not include aerosols or CCN effect on clouds. This version takes the least calculation cost in the four versions.

The “Cloud bin model” version is the newest and the main version in this study. The bin-type cloud microphysical scheme and the radiation scheme, “mstrn-x” are adapted to JMA-NHM. The size ranges for CCN and hydrometers are illustrated in Fig. 2.3. Different from the "Proto type model", this version was highly optimized for a three-dimensional simulation including all the bin-type water and ice cloud processes for a massive

computational system with the code parallelization technique of Message-Passing Interface (MPI) parallelism.

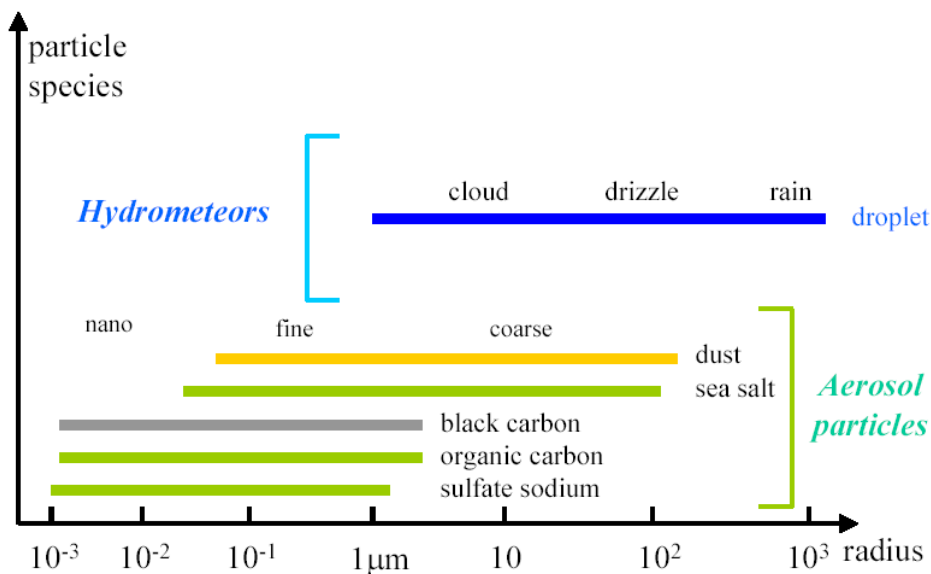


Figure 2.2 The profile of size ranges covered with aerosols and hydrometeors, adopting the bin-type both aerosol and cloud schemes.

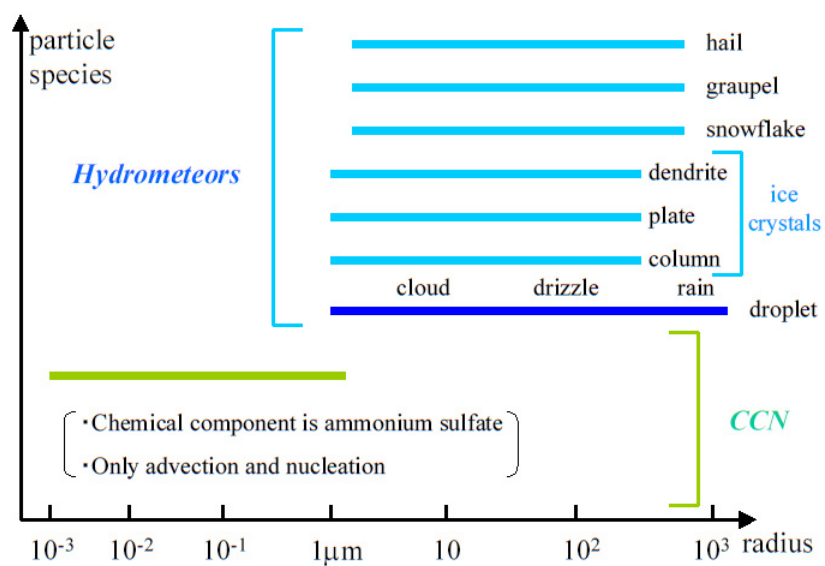


Figure 2.3 As in Figure 2.2 except for covered with CCN and hydrometers, adopting only the bin-type cloud scheme.

2.3 Setup of numerical experiments

Numerical simulations are carried out in this study in a region around the East China Sea

within a radius of 1,400 kilometers and whose center is located in the sea near the Kyushu region, projected on a map of Lambert coordinates (Fig. 2.4). The JMA meso-analysis dataset, with horizontal grid size of 10 km, 20 vertical layers, and time step of 6 hour intervals, is used for initialization and nesting of dynamical variables, i.e., horizontal velocities, temperature, and relative humidity. The horizontal grid size of the model is set at 7 km (for 202 grid points). A terrain-following vertical coordinate is introduced, and then 38 vertical atmospheric layers up to 10,910 m with intervals increasing with altitude (40 m for the bottom layer to 580 m for the top layer) in the two versions based on MRI/NPD-NHM and 40 vertical layers up to 22,600 m (40 m for the bottom layer to 1,120 m for the top layer) in the two versions based on JMA-NHM are employed. The time step is taken to be 20 seconds for dynamical process and to be a variable time interval for the diffusion growth, evaporation, sublimation process in the bin-type cloud microphysical scheme.

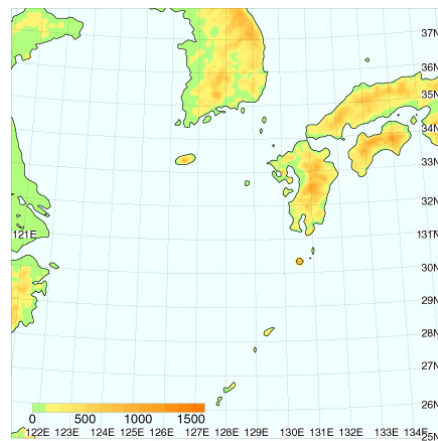


Figure 2.4 Domain targeted by the numerical simulations. The radius is 1,400 kilometers, projected on a frame of Lambert coordinates. The color contour shows the orography.

2.4 Observation data compared with simulated results

Variety of observation data is used in the present study to be compared with model simulation results.

The Moderate Resolution Imaging Spectroradiometer (MODIS) is a key instrument aboard the Terra satellite. Terra crosses the equator from north to south at the local time of 10:30am. Terra/MODIS has a viewing swath width of 2,330 km, acquiring data in 36 spectral bands ranging in wavelength from 0.4 μm to 14.4 μm at three spatial resolutions, 250m, 500m, and 1,000m. Many data products derived from MODIS observations give characteristics of land, ocean and atmosphere that can be used for studies of processes and trends on local to global scales.

Terra/MODIS aerosol products derived by the algorithm of *Higurashi et al.* [2002] consist of aerosol optical thickness at 500 nm, Ångström exponent, and aerosol type. Aerosols are classified into four aerosol species (soil dust, carbonaceous, sulfate, and sea salt), based on Ångström exponent and blue-spectral radiative absorptivity. These aerosol data is only calculated in clear (not cloudy) atmosphere on the sea. Terra/MODIS products from the algorithm of *Nakajima and Nakajima* [1995] and *Nakajima et al.* [2005] include cloud optical thickness, LWP, droplet effective radius near the cloud top, cloud top temperature, and cloud top altitude. Pixels in which there are ice clouds are excluded from cloud retrieval process.

Airborne measurement data were taken in the APEX-E3 experiment, which is one of series of JST/CREST/APEX regional experiments [Nakajima et al., 2001]. A Cessna 404 aircraft took flights on 17, 20, 22, 26, 29, and 31 March and 2, 5, 8, 9, 10, 12, and 13 April 2003 to measure the CCN concentration and cloud droplet concentration by a CCN counter, Model ACN-1000, SIGMATEC, and a particle counter, Model FSSP-100, PMS [Adhikari et al., 2005]. An accurate comparison of the result of aircraft measurements with the simulation result is difficult because the observation time and flight courses are irregular. Also the measured airmass by in situ instruments is much smaller than the spatial resolution of the model. Thus, we take a reasonably simple method for a qualitative comparison in this study with the following procedure: Firstly we select flight legs falling in a domain within a radius of ± 2 degrees in latitude and longitude whose center is located at 130 °E, 30 °N. Then, the domain averages of the simulated variables are compared with the observed values.

We also use 1-hr precipitation analysis data from JMA's Radar-Automated Meteorological Data Acquisition System (AMeDAS) around the Japan Islands with the horizontal grid size of 2.5 km.

2.5 General weather condition of the targeted days

Three days, 2 April 2003, 8 April 2003, and 13 March 2005, which have different weather condition, are selected as targeted days for numerical experiments. Images of Terra/MODIS cover the targeted region roughly at noon (0300 UTC) on these days. Measurements by aircraft to the CCN concentration were taken on 2 April and 8 April 2003.

At 0000 UTC 2 April 2003, there is a low with a stationary front extended east and west around a latitude of 30°N and the southern sea of Japan (Fig. 2.5(a)). Surface synoptic observations in the calculation domain indicate that almost all parts of the area were covered with clouds as in the satellite imagery (Fig. 2.6(a)), for example, cirrus over the Korean Peninsula and the Japan Sea, and large thick clouds on the east coast of China, and low clouds over the East China Sea around the Kyushu Island.

On 8 April 2003, a migrating low was located in the Japan Sea near the Korean Peninsula. A row of thick convective clouds was developed from the center of Japan Sea to the Naha

region and Taiwan by the cold front associated with the low (Fig. 2.5(b)). Very thin clouds covering the wide area of the domain are found in the satellite observation shown in Fig. 2.6(b).

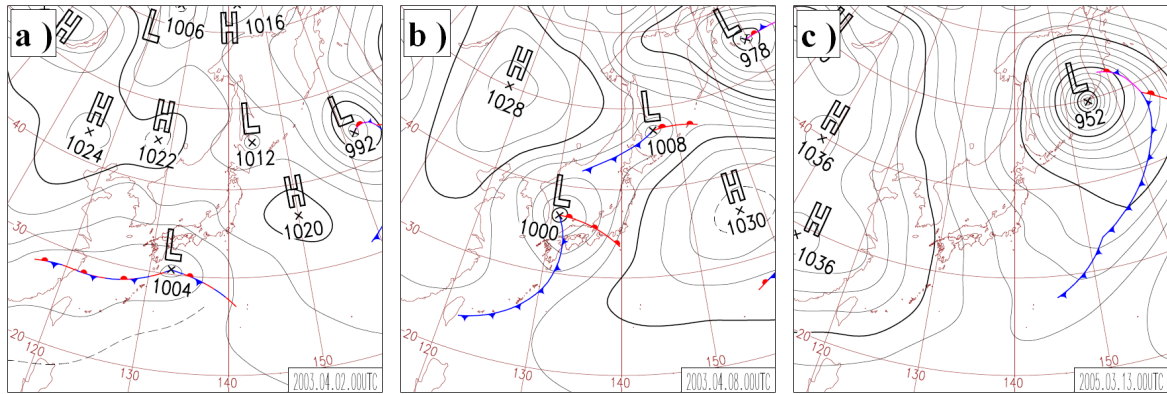


Figure 2.5 JMA surface weather charts at 0000 UTC (a) on 2 April 2003, (b) on 8 April 2003, and (c) on 13 March 2005.

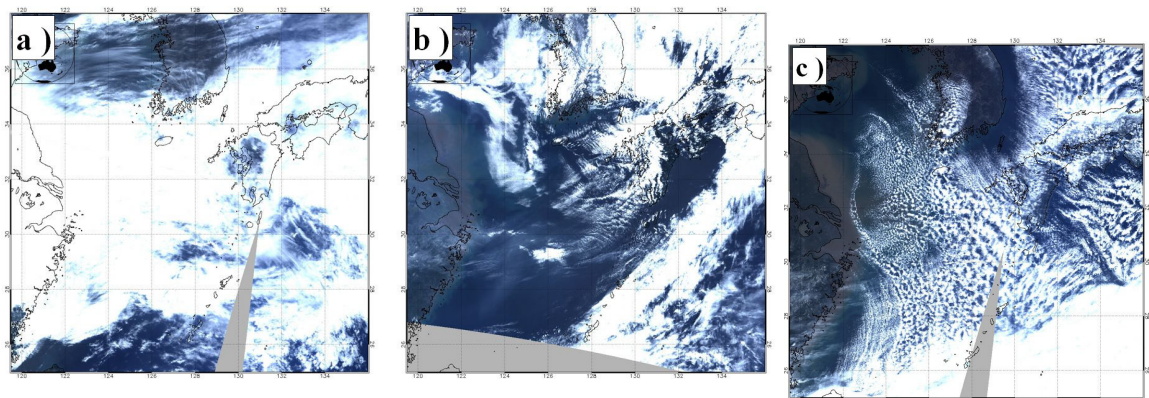


Figure 2.6 Terra/MODIS RGB images with 1km resolution (a) on 2 April 2003, (b) on 8 April 2003, and (c) on 13 March 2005.

A typical distribution of the atmospheric pressure in winter of this region was seen on the surface weather map at 0000 UTC 13 March 2005 (Fig. 2.5(c)), with low and high pressure systems located in the eastern sea and in the western land and isobars extending from north to south. Convective pattern with low cumuli and a row of thick clouds associated with a cold front covered the southeast area of the domain as shown in Fig. 2.6(c). Surface synoptic observations indicate a snowfall at the Cheju Island, the Kyushu and Shikoku Regions.

Appendix 2A: The basic dynamics equations

In MRI/NPD-NHM and JMA-NHM, the following fully compressible equations considering a map factor are adopted as the basic equations [Saito, 1997]. The momentum equations are given as flux forms:

$$\frac{\partial}{\partial t} \left(\frac{\rho u}{m_f} \right) + Adv. \left(\frac{\rho u}{m_f} \right) + \frac{\partial p}{\partial x} = Crv. \left(\frac{\rho u}{m_f} \right) + Cor. \left(\frac{\rho u}{m_f} \right) + Dif. \left(\frac{\rho u}{m_f} \right), \quad (2A.1)$$

$$\frac{\partial}{\partial t} \left(\frac{\rho v}{m_f} \right) + Adv. \left(\frac{\rho v}{m_f} \right) + \frac{\partial p}{\partial y} = Crv. \left(\frac{\rho v}{m_f} \right) + Cor. \left(\frac{\rho v}{m_f} \right) + Dif. \left(\frac{\rho v}{m_f} \right), \quad (2A.2)$$

$$\frac{\partial}{\partial t} \left(\frac{\rho w}{m_f} \right) + Adv. \left(\frac{\rho w}{m_f} \right) + \frac{1}{m_f} \left(\frac{\partial p}{\partial z} + \rho g \right) = Crv. \left(\frac{\rho w}{m_f} \right) + Cor. \left(\frac{\rho w}{m_f} \right) + Dif. \left(\frac{\rho w}{m_f} \right), \quad (2A.3)$$

$$m_f \equiv \left(\frac{\cos \varphi}{\cos \varphi_1} \right)^{c-1} \left(\frac{1 + \sin \varphi_1}{1 + \sin \varphi} \right)^c; \quad c = \left(\frac{\cos \varphi_1}{\cos \varphi_2} \right) / \ln \left\{ \frac{\tan \left(\frac{\pi}{4} - \frac{\varphi_1}{2} \right)}{\tan \left(\frac{\pi}{4} - \frac{\varphi_2}{2} \right)} \right\}, \quad (2A.4)$$

where u , v and w are the east and west, north and south and vertical components of the velocities respectively, p is the pressure, g is the gravitational acceleration, ρ is the density including hydrometeors; m_f is defined as the map factor, and φ_1 and φ_2 are the standard latitudes and φ is the latitude. *Adv.*, *Crv.*, *Cor.*, and *Dif.* stand for the advection, curvature, Coriolis, and diffusion processes, respectively. The thermodynamic equation is given as follows:

$$\frac{\partial \theta}{\partial t} + Adv. \theta = \frac{Q}{C_p \Pi} + Dif. \theta, \quad (2A.5)$$

$$\Pi \equiv \left(\frac{p}{p_0} \right)^{R/C_p}, \quad (2A.6)$$

where θ is the potential temperature, Q is the diabatic heating rate, C_p is the specific heat of dry air at constant pressure, Π is defined as the Exner function, p_0 is the standard pressure, and R is the gas constant for dry air. The continuity equation is given as,

$$\frac{\partial \rho}{\partial t} + m_f^2 \left\{ \frac{\partial}{\partial x} \left(\frac{\rho u}{m_f} \right) + \frac{\partial}{\partial y} \left(\frac{\rho v}{m_f} \right) \right\} + \frac{\partial}{\partial z} (\rho w) = Prc. \quad (2A.7)$$

where *Prc.* is the term corresponding to the gravitational settling of the hydrometeors.

A non-hydrostatic model can treat the convection explicitly and introduce a high horizontal resolution. Thus, the model is suitable for a cloud resolving simulation and can agree with the

demand of this study. However, since the change of density in time is calculated explicitly and sound waves are included in the solutions, a special treatment is needed to prevent the inflation of sound waves by restricting the maximum time-step. MRI/NPD-NHM has prepared two schemes to solve this problem: one is a scheme that treats waves implicitly in horizontal and implicitly in vertical (HI-VI scheme) and another is a scheme that treats waves explicitly in horizontal and implicitly in vertical (HE-VI scheme).

Appendix 2B: Bin-type cloud microphysical scheme

The bin-type cloud microphysical scheme in this study is based on the Hebrew University Cloud Model (HUCM) [e.g., *Khain and Sednev, 1996*]. This scheme represents nucleation from CCN to droplets, nucleation to ice crystals, diffusion growth, evaporation, sublimation, droplet freezing (immersion freezing), melting, and coagulation growth processes for seven hydrometeors (water droplets, ice crystals (plate, column, dendrite), snowflakes, graupels, and hails). The graupels and hails are both characterized as rimed particles, but their bulk densities are different.

The basic conservation equation of hydrometeors is given as,

$$\frac{\partial f_{i,k}}{\partial t} + Adv.(f_{i,k}) - Drp.(f_{i,k}) = - \left[\frac{\partial f_{i,k}}{\partial t} \right]_{microphysics}, \quad (2B.1)$$

where $f_{i,k}$ is the size distribution function of hydrometeors in size bin category whose subscripts, i and k ($=1, \dots, 33$), denote the type of hydrometeor and the bin-size number; The term $[]_{microphysics}$ is the rate of change due to the cloud microphysical processes.

The nucleation process from CCN to cloud droplets is calculated owing to the following theories: If there is a droplet containing a soluble part in the equilibrium state with its environment, the supersaturation around the droplet is described by the Köhler equation [e.g., *Rogers and Yau, 1989*]:

$$S_w = \frac{A}{r_w} - \frac{Br_{ccn}^3}{r_w^3}, \quad (2B.3)$$

$$A \approx \frac{3.3 \times 10^{-5}}{T} \text{ (cm)}; \quad B \approx \frac{4.3\nu}{M_{ccn}} \left(\frac{4\pi\rho_{ccn}}{3} \right) \text{ (cm)}, \quad (2B.4)$$

where S_w is the supersaturation over water, r_w is the radius of the droplet, r_{ccn} is the radius of the CCN. About (2B.4), T is the temperature, ν is the Van't Hoff factor [e.g., *Low, 1969*], M_{ccn} is the molecular weight, and ρ_{ccn} is the density of CCN. The composition of CCN is assumed to be uniform. In equation (2B.4), the maximum supersaturation for any droplet radius is determined by the condition, $dS/dr = 0$, and the maximum is defined as S_{crit} ,

$$S_{crit(w)} = \frac{2A}{3r_{crit}}, \quad r_{crit(w)} = \sqrt{\frac{3Br_{ccn}^3}{A}}, \quad (2B.5)$$

where $r_{crit(w)}$ is the droplet radius that is calculated by substituting $S_{crit(w)}$ for S_w in (2B.3). Then, the radius of CCN that is one-to-one corresponding to $S_{crit(w)}$ is calculated by (2B.5),

$$r_{crit(CCN)} = \left(\frac{4}{27} \frac{A^3}{B} \frac{1}{S_{crit(w)}} \right)^{1/3}, \quad (2B.6)$$

We assume that all CCN of which radius is larger than the minimum radius calculated by (2B.6) is converted to droplets.

Calculation of the nucleation process to ice crystals is based on the following parameterization suggested by *Meyers et al.* [1992], which relates deposition and condensation freezing due to Ice Nuclei (IN),

$$N_d = 10^{-3} \exp(-0.639 + 12.96S_{ice})(m^{-3}), \quad (2B.7)$$

where N_d is the number concentration of generated ice crystals and S_{ice} is the supersaturation over ice. The type of generated ice crystals depends on the environmental temperature [*Takahashi et al.*, 1991].

Then the diffusion growth of hydrometeors is calculated as in [*Khain and Sednev*, 1996]: First, hydrometeor's mass change by condensation, evaporation, deposition, and sublimation is given analytically as follows [e.g., *Rogers and Yau*, 1989],

$$\frac{dm_w}{dt} = \frac{4\pi r_w S_w}{F_w}, \quad \frac{dm_{ice}}{dt} = \frac{4\pi C_{ice} S_{ice}}{F_{ice}}, \quad (2B.8)$$

$$F_w = \frac{R_v T}{e_{s(w)} D_v} + \frac{L_w}{K_\alpha T} \left(\frac{L_w}{R_v T} - 1 \right), \quad F_{ice} = \frac{R_v T}{e_{s(ice)} D_v} + \frac{L_{ice}}{K_\alpha T} \left(\frac{L_{ice}}{R_v T} - 1 \right), \quad (2B.9)$$

where m_w and m_{ice} are the masses of hydrometeors whose subscripts, w or ice , denote water droplets or other 6-type ice particles, C_{ice} is the shape factor of ice hydrometeors [*Khain and Sednev*, 1996], R_v is the gas constant of the water vapor, $e_{s(w)}$ and $e_{s(ice)}$ are the saturation vapor pressure for water and ice, D_v is the diffusivity of the water vapor, L_w and L_{ice} are the specific latent heat of vaporization for water and sublimation for ice, and K_α is the thermal conductivity of air. In (2B.8) and (2B.9), the effects of the solution and curvature are neglected assuming that they are very small.

(2B.9) is replaced with a differential equation of supersaturation, considering the changes of water vapor and temperature due to condensation and evaporation on a grid as follows,

$$\frac{dS_w}{dt} = -P_1 S_w - P_2 S_{ice}, \quad \frac{dS_{ice}}{dt} = -R_1 S_w - R_2 S_{ice}, \quad (2B.10)$$

$$P_1 = \frac{e}{e_{s(w)}} \left(\frac{1}{q(0.622 + q)} + \frac{L_w^2}{C_p T^2 R_v} \right) \int_0^\infty \frac{4\pi r_w}{F_w} f_{i=w,k} dm,$$

$$P_2 = \frac{e}{e_{s(w)}} \left(\frac{1}{q(0.622 + q)} + \frac{L_{ice} L_w}{C_p T^2 R_v} \right) \sum_{i=ice} \int_0^\infty \frac{4\pi C_{ice}}{F_{ice}} f_{i,k} dm,$$

$$R_1 = \frac{e}{e_{s(ice)}} \left(\frac{1}{q(0.622 + q)} + \frac{L_{ice} L_w}{C_p T^2 R_v} \right) \int_0^\infty \frac{4\pi r_w}{F_w} f_{i=w,k} dm,$$

$$R_2 = \frac{e}{e_{s(ice)}} \left(\frac{1}{q(0.622 + q)} + \frac{L_{ice}^2}{C_p T^2 R_v} \right) \sum_{i=ice} \int_0^\infty \frac{4\pi C_{ice}}{F_{ice}} f_{i,k} dm,$$

where e is the vapor pressure, q is the mixing ratio of the water vapor, $f_{i=w,k}$ is the size distribution function of water droplets, and $\sum_{i=ice}$ denotes the sum of values for 6-type ice particles.

In the actual computation, numerical integration of (2B.8) and (2B.10) is calculated with a time-interval Δt_m to calculate the evolution of the size distribution function f_w . This Δt_m is decided, provided that $r\Delta r$ is constant in the discretized form of (2B.7), as a typical timescale needed for a change in the condensation or evaporation of hydrometeors. Numerical integration of (2B.8) and (2B.10) is continued as far as the sum of Δt_m is less than the time interval for the dynamical process.

The freezing process of water droplets (immersion freezing) is based on two parameterizations. Selection from one parameterization to other depends on the environmental temperature. If the temperature is larger than 235.15 K, the parameterization by *Ovtchinnikov and Kogan* (2000) is used. In the parameterization, a number concentration of activated immersion nuclei per unit volume of liquid water is given by the following equation:

$$N_{im} = N_{im0} (0.1T)^{4.4}, \quad (2B.11)$$

where N_{im0} is the number concentration of all immersion nuclei per unit volume of liquid water. The type of generated ice particles by freezing depends on the size of frozen water droplets. The frozen water droplets whose radii are smaller than 200 μm are converted to plate-like ice crystals of corresponding masses and the others are transformed to hails.

If the temperature is smaller than 235.15 K, the parameterization by *Bigg* (1953) is selected. In the parameterization, the freezing probability is assumed proportional to the droplet mass. The decrease in the size distribution function of water droplets is calculated as:

$$\frac{1}{f_{i=w,k}} \frac{\partial f_{i=w,k}}{\partial t} = -10^{-4} m_w \exp(-0.66T)(s^{-1}g^{-1}). \quad (2B.12)$$

The number of the same type of ice particles generated by (2B.11) depends on the size of frozen water droplets. Melting of ice hydrometeors is based on a simple parameterization. All ice hydrometeors are converted to water droplets of corresponding masses when the environmental temperature becomes larger than 273.15 K.

The coalescence growth of hydrometeors is calculated by the following equation [Pruppacher and Klett, 1997; Khain et al., 2000],

$$\frac{\partial f(m)}{\partial t} = 2 \int_0^{m/2} f(m-m')K(m, m-m')f(m')dm' - \int_0^\infty f(m)K(m, m')f(m')dm', \quad (2B.13)$$

$$K(m, m') = \pi \{r(m) - r(m')\}^2 |V(m) - V(m')| E_{col}(m, m') E_{coal}(m, m'), \quad (2B.14)$$

where V is the terminal velocity of hydrometeors, E_{col} is the collision efficiency, and E_{coal} is the coalescence efficiency factor. The type of the coagulated particle depends on the type of parent particles and the environmental temperature. The correspondence is listed in Fig. 2B.1. In the numerical computation, a flux-type scheme by Bott [1998] is used to prevent the generation of artificially large droplets by a numerical error.

Y \ X	DR	IC	SN	GR	HA
DR	DR	GR/HA	GR/HA	GR/HA	GR/HA
IC	IC	SN	SN	IC	IC
SN	SN	SN	SN	SN	SN
GR	GR/HA	GR/HA	GR	GR	GR/HA
HA	GR/HA	GR/HA	GR/HA	GR/HA	HA

Figure 2B.1 Coagulation interactions between hydrometeors. *DR*, *IC*, *SN*, *GR*, and *HA* indicates water droplets, ice crystals, snow flakes, graupels, and hails, respectively. The line category expresses generated hydrometeors on condition that the mass of *Y* particle is larger than that of *X* particle, whereas the column category shows the condition that the mass of *Y* particle is smaller than that of *X* particle. *GR/HA* indicates that generation of graupels or hails depends on the environmental temperature.

Appendix 2C: CCN in the bin-type cloud microphysical scheme based on HUCM

In this bin-type cloud microphysical scheme based on the HUCM, The basic conservation equation of Cloud Condensation Nuclei (CCN) is given as,

$$\frac{\partial f_{ccn,l}}{\partial t} + Adv.(f_{ccn,l}) = - \left[\frac{\partial f_{ccn,l}}{\partial t} \right]_{nucleation} + Dif.(f_{ccn,l}), \quad (2C.1)$$

where $f_{ccn,l}$ is the size distribution function of CCN in the size bin category whose subscript, l denote the bin-size number and the term $[]_{nucleation}$ is the rate of reduction due to a conversion process to cloud droplets. The source of CCN is only due to inflow from the lateral boundaries and the sink is due to an outflow at the lateral boundaries and consumption by nucleation. The CCN's terminal fall velocities are neglected.

As for activation of CCN (nucleation to droplets) process, the critical radius of the CCN is calculated based on (2B.4), (2B.5), and (2B.6), which depends on the chemical composition and physical properties of the aerosol (CCN) and the supersaturation of the environment obtained by temperature and the mixing ratio of water vapor. All CCN of which radius is larger than the minimum radius calculated by (2B.6) is converted to droplets in each time-step. Ammonium sulfate ((NH₄)₂SO₄) as the chemical composition is assumed in this study.

The size distribution function of CCN in the size bin is one of the model variables and is essential to the calculation of the nucleation process of droplets as indicated in Appendix 2B. In HUCM, an initial size distribution function of CCN in size bin category whose number is l is assumed as a form given as this equation:

$$f_{ccn,l} = 1.5CK \left(\frac{4}{27} \frac{A^3}{B} \frac{1}{r_{ccn,l}^3} \right)^K, \quad (2C.2)$$

where C and K are the constants for a given type of air-mass [Pruppacher and Klett, 1997] and, A and B are indicated in (2B.4). In the original study of Khain and Sednev [1996] an initial field of CCN is assumed as the concentration decreasing exponentially with height and uniform horizontally.

On the other hand, we assume an inhomogeneous initial field and a lateral boundary condition by introducing a nesting method. The CCN data for nesting is given by the result of a global aerosol transport and radiation model, SPRINTARS [e.g., Takemura et al., 2000], for five tropospheric aerosols (organic carbonaceous, black carbonaceous, soil dust, sulfate and sea salt). Among these aerosols, organic carbonaceous, sulfate and sea salt are assumed to be hygroscopic and serve as CCN.

A method of converting the concentrations of the hygroscopic aerosols to the size distribution function of CCN at grid points is as follows: the concentration of each hygroscopic aerosol is prepared by SPRINTARS in the form of a bulk number concentration of dry hygroscopic aerosol particles, and then the bulk number concentration is converted to a size distribution function by assuming a function depending on the aerosol type. Size

distributions of organic carbonaceous and sulfate are assumed to depend on log-normal type distribution. As a result, the size distribution function of CCN is given as

$$f_{ccn,l} = \frac{N_{OC}}{\sqrt{2\pi}\sigma_{OC}} \exp\left[-\frac{1}{2}\left\{\frac{\ln(r_{ccn,l}/r_{OC})}{\sigma_{OC}}\right\}^2\right] + \frac{N_{SU}}{\sqrt{2\pi}\sigma_{SU}} \exp\left[-\frac{1}{2}\left\{\frac{\ln(r_{ccn,l}/r_{SU})}{\sigma_{SU}}\right\}^2\right], \quad (2C.3)$$

where suffix "OC" and "SU" represent parameters for organic and sulfate aerosols, respectively, N is the number concentration of aerosols calculated by SPRINTARS, r is the mode radius, and σ is the standard deviation of the size distribution. Parameters are assumed as $r_{OC} = 0.1 \mu\text{m}$ and $\sigma_{OC} = 1.8$ for carbonaceous aerosols, and $r_{SU} = 0.0695\mu\text{m}$ and $\sigma_{SU} = 2.03$ for sulfate. The size distribution of sea salt aerosols is assumed to be given by

$$f_{ccn,l} = 1.5N_{SA}K\left(\frac{B_{SA}}{B}\frac{r_{SA}}{r_{ccn,l}^3}\right)^K, \quad (2C.4)$$

where N_{SA} is the number concentration of sea salt from SPRINTARS and B_{SA} corresponds to B defined in (2B.4) whose Van't Hoff factor, molecular weight and density are given as those of the sea salt aerosols, and $r_{SA} = 0.1 \mu\text{m}$. Finally, the sum of (2C.3) and (2C.4) is used as the size distribution function of CCN.

External reference values are used to calculate an external value at the grid point outside and adjacent to the lateral boundary, because JMA-NHM and MRI/NPD-NHM use the Arakawa C grid structure as the horizontal discretization. The external value at the next time step is calculated in the following form [Ikawa and Saito, 1991]:

$$f_{out}^{\tau+1} = \beta f_{EXT}^{\tau} + (1 - \beta)(2f_{in}^{\tau} - f_{in-1}^{\tau}) \quad \text{for } U \geq 0, \quad (2C.5)$$

$$f_{out}^{\tau+1} = \beta f_{EXT}^{\tau} + (1 - \beta)f_{out}^{\tau-1} \quad \text{for } U < 0, \quad (2C.6)$$

where f_{out} and f_{in} are the external and inertial distribution functions at grid points adjacent to the lateral boundary, f_{in-1} is the function at grid points inside and next to the grid at which f_{in} is, and f_{EXT} is the external reference value; β is a weighting parameter, U is the normal wind component to the lateral boundary, and τ is the time-step.

Appendix 2D: Code parallelization and calculation cost

A nested simulation including all water and ice cloud processes in the bin-type cloud microphysical scheme can be computed on a massive computational server using a code parallelization technique with 1-dimensional (y) domain decomposition with Message-Passing Interface (MPI) parallelizm. As an example of the computational time, about 16 hours is taken for 1620 times of time-integration in a nested simulation for the typical calculation domain (202 * 202 * 40 grids) with 32 processors (4 nodes) on a

HITACHI SR11000/J1 at Tokyo University.

Almost all the actual computational time is consumed to compute the advection processes of CCN and hydrometeors and the cloud microphysical process. The efficiency of parallelization is much lower than that of a bulk-type cloud model because a heterogeneous distribution of cloudy grid produces a large difference in actual computational time that each processor needs to calculate those processes, so that processors allocated to clear sky domain need to wait for finishing of computation by processors for cloudy domain in each time step. Then, we introduced a technique to estimate the distribution of cloudy grids from former simulated results in the same condition or from an interpolation of the nesting data, and then to optimize computational domain allocation to each processor so as to minimize the total waiting time. Figure 2D.1 shows an example that the computational efficiency was extremely improved by the technique. In the case of Fig. 2D.1(a), the computational domains are allocated uniformly to each processor. In such allocation, some processors need to process many cloudy grids and other many processors are allocated clear grids, so that the processors in the clear sky domains have much waiting time. The total CPU time for 3 hours integration was about 40,600 seconds. In the case of Fig. 2D.1(b), the optimum technique was used, by which more processors than in case of Fig. 2D.1(a) are allocated to process the cloudy domain to reduce the waiting time of the processors allocated to the clear sky domains. The total CPU time for 3 hours integration was about 16,600 seconds.

This technique, however, has some problems: One problem is that the technique becomes inefficient as the integration time becomes larger, because the cloudy region changes from the initial field. Other problem is that it is difficult to adopt it to 2-dimensional (x-y or y-z) domain decomposition. We need to find better technique to save computational time in future.

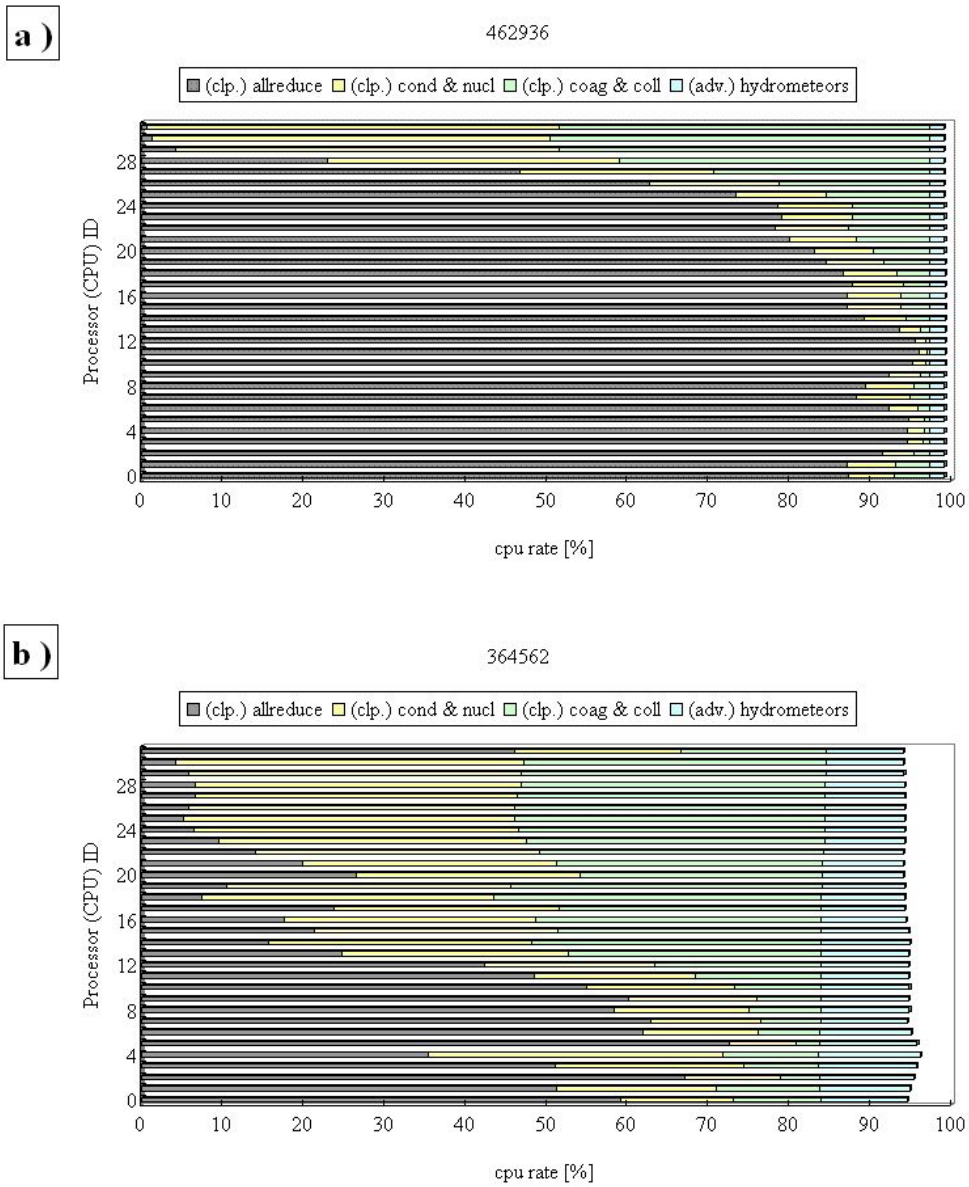


Figure 2D.1 The percentages of CPU time used by each module on condition (a) that the computational domains are arranged uniformly and (b) that the sizes of computational domains are optimized. *(clp.)allreduce*, *(clp.)cond&nucl*, *(clp.)coag&coll*, and *(adv.)hydrometeors* mean CPU rates by modules for waiting for finishing of computation by other processors, calculating condensation, sublimation, evaporation, and nucleation processes, calculating coagulation growth process, and calculating advections of hydrometeors and CCN, respectively.

Chapter 3 Aerosol distribution simulated by a nesting method

3.1 Introduction

As discussed in the preceding sections, aerosols are closely related with clouds. Accurate simulation of the aerosol field is one of important research subjects to which the cloud resolving model can contribute. Most of past studies with bin-type cloud microphysical models introduced simple initialization and lateral boundary condition of the aerosols or CCN concentration for an ideal simulation as reviewed in subsection 2.2.4 without paying much attention to the aerosol field which is supposed to be assumed in the atmospheric condition they study.

In this chapter we closely investigate how the aerosol field can be simulated by the present nonhydrostatic regional model. For this purpose the version, “Aerosol and cloud bin model (ACBM)” described in chapter 2 is used to perform a nesting run for aerosol and cloud field simulation. The result of simulation is compared with the original result of SPRINTARS with CCSR/NIES-AGCM interpolated at the model grids and is also compared with the Terra/MODIS aerosol product by the algorithm of *Higurashi et al.* [2002]. The calculation starts from 1800 UTC 7 April 2003, and the simulated fields at 0300 UTC 8 April 2003 are used for analysis.

Figure 3.1 shows horizontal distributions of LWP at 0300 UTC and 1-hr precipitation amount from 0200 to 0300 UTC 8 April 2003, simulated by ACBM. Figure 3.2 shows horizontal distributions of mass concentrations of dust, sea salt, and sulfate aerosols near surface (roughly 60 m above surface on the terrain-following vertical coordinate). There was hardly any emission of dust aerosols in the domain, so that the dust aerosols were almost attributed to transported dust particles from deserts in the interior of the Eurasian Continent, such as the Gobi and Taklamakan deserts. In the case of mineral dust aerosols transportation from the continent, the concentration of dust aerosols is usually large in the middle layer of the troposphere where the prevailing westerlies are dominant. The concentrated dust aerosols in the middle layer were thus simulated to descend to near the surface owing to the downdraft due to the high pressure system behind the cold front, whereas the concentration along the cold front was clearly decreased owing to impaction scavenging by precipitation shown as in Fig. 3.1. As for sea salt aerosols, the magnitude of emission from sea surface depends on the wind velocity on the sea surface. Thus, large emission occurred in the eastern part of the domain owing to the strong surface wind associated with the cold front. An increase in the concentration by the large emission was partly canceled by the impaction scavenging by precipitation and consumption with nucleation to droplets. The maximum value existed on the part of the Japan Sea near the center of the low pressure system where there was no cloud and precipitation shown as in Fig. 3.1. The sulfate aerosols were dominant in the western part

of the domain. Most of sulfate aerosols were from an industrial area on the east part of the China which is out of the domain, and then their advection are influenced by the flow in the lower troposphere while they were transported eastward. The distribution of black and organic carbon aerosols was similar to that of the sulfate aerosols because these carbonaceous aerosols were from the industrial area also.

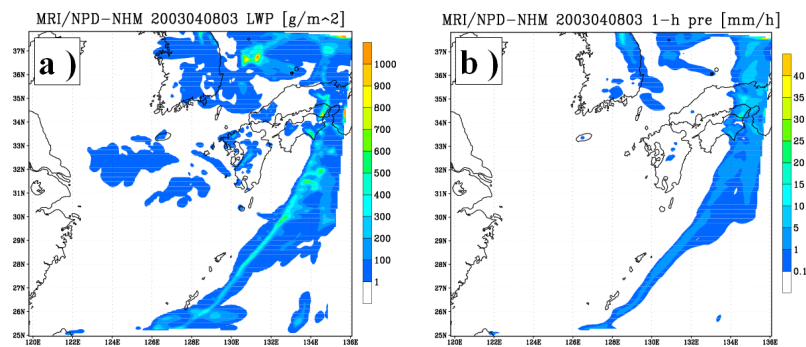


Figure 3.1 The horizontal distributions of (a) liquid water path (g/m^2) at 0300 UTC and (b) 1-h precipitation amount (mm/h) from 0200 UTC to 0300 UTC 8 April 2003. These are simulated by the version, “Aerosol and cloud bin model”.

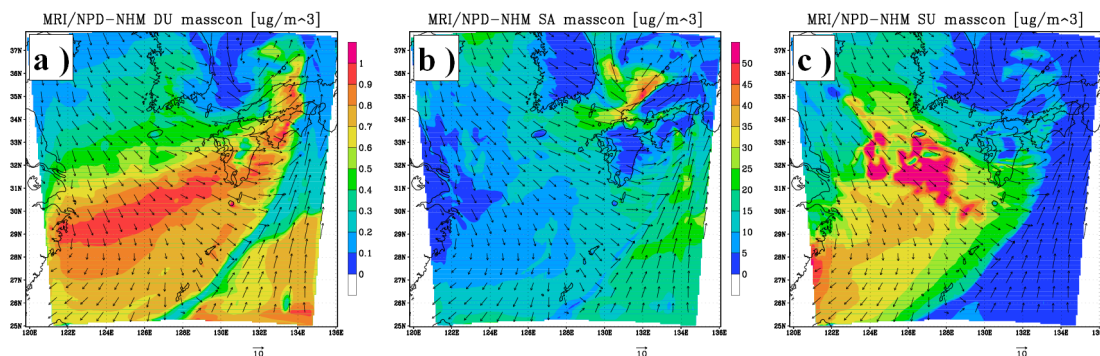


Figure 3.2 The simulated horizontal distributions of surface mass concentration of (a) dust, (b) sea salt, and (c) sulfate aerosols at 0300 UTC 8 April 2003. These are simulated by the version, “Aerosol and cloud bin model”.

3.2 Comparison with the result of SPRINTARS

Figure 3.3 shows the horizontal distributions of mass concentrations of aerosols near the surface by simulation of the original SPRINTARS coupled with CCSR/NIES-AGCM with a horizontal resolution of T106 interpolated at the model grids at 0300 UTC on 8 April 2003. The distribution of sulfate aerosols is similar to that of “Aerosol and cloud bin model” (Fig. 3.2), but distributions of dust and sea salt aerosols are different from those of ACBM.

Most of sulfate aerosols were from the source area located outside the domain, so that the distribution resulted from advection of the aerosols in the initial field and from the lateral boundaries introduced by the nesting method. Horizontal advection rather than vertical advection was important to decide the distribution of sulfate aerosol concentration near surface because sulfate aerosols were concentrated near surface. Thus, the distribution of sulfate aerosols near surface was well simulated as the nested model from the original data calculated by SPRINTARS. As for dust aerosols, the source is also out of the domain. Vertical advection, however, played an important role of calculating the profile of the concentration near surface because concentrated dust aerosols in the middle layer have to descend to near surface in the simulation. Precision to reproduce the dynamical field by ACBM model is probably better than that by CCSR/NIES-AGCM, so that the nested model properly reproduced the distribution of dust aerosols near surface, though the distribution was different from that by SPRINTARS with CCSR/NIES-AGCM. Emission of sea salt aerosols is only from sea surface and its magnitude depends on the horizontal wind velocity near sea surface. In the both simulations, sea salt aerosols were mainly produced and concentrated near the cold front because strong wind near the cold front caused large emission. An area of maximum concentration existed in the part of the Japan Sea in the simulation by ACBM because of the reason given in the former section, whereas such area is in the part of the Pacific by the original SPRINTARS with a rough cloud resolving and aerosol scavenging simulation. Since the nested model can simulate better high-resolution structure of the cloud system and hence better impactation scavenging process, the nested model is expected to produce more accurate distribution of sea salt aerosols, though degree of accuracy is needed to be verified by a comparison with observation.

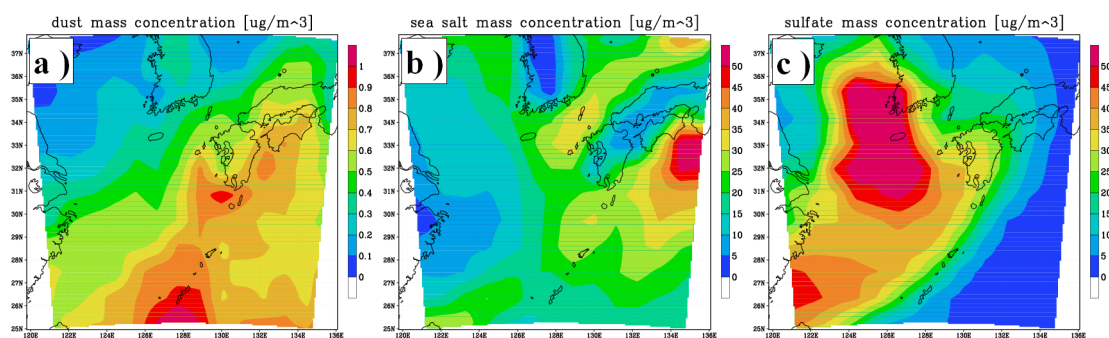


Figure 3.3 As in Figure 3.2 except for simulated by the original SPRINTARS with CCSR/NIES-AGCM.

3.3 Comparison with satellite data

Figure 3.4 shows horizontal distributions of aerosol optical thickness (AOT) simulated by

ACBM and observed by satellite at 0300 UTC 8 April 2003. The satellite retrieval data are given from aerosol products by the algorithm of *Higurashi et al.* [2002]. The optical thickness due to aerosols at a wavelength of 0.5 μm in the simulation is calculated with the following formula [*Takemura et al.*, 2000, equation B1],

$$\tau = \sum_i \left(\frac{3}{4} \sum_{k=1}^{k_{\max}} \frac{Q_{\text{ext}}(i, k) q_a(i, k) \Delta p(k)}{\rho_a(k) r_a(i, k) g} \right), \quad (3.1)$$

where $Q_{\text{ext}}(i, k)$ is the extinction efficiency factor as a function of the size bin i , aerosol type, and relative humidity at the k -th layer, q_a is the mixing ratio of the aerosol particle, Δp is the pressure difference between the upper and the lower boundaries at each vertical layer, ρ_a is the density of the aerosol particle as a function of the aerosol type and relative humidity, r_a is the radius of the aerosol particle, and g is the gravitational acceleration. The Mie theory is applied to calculate the efficiency factor of the aerosol particles.

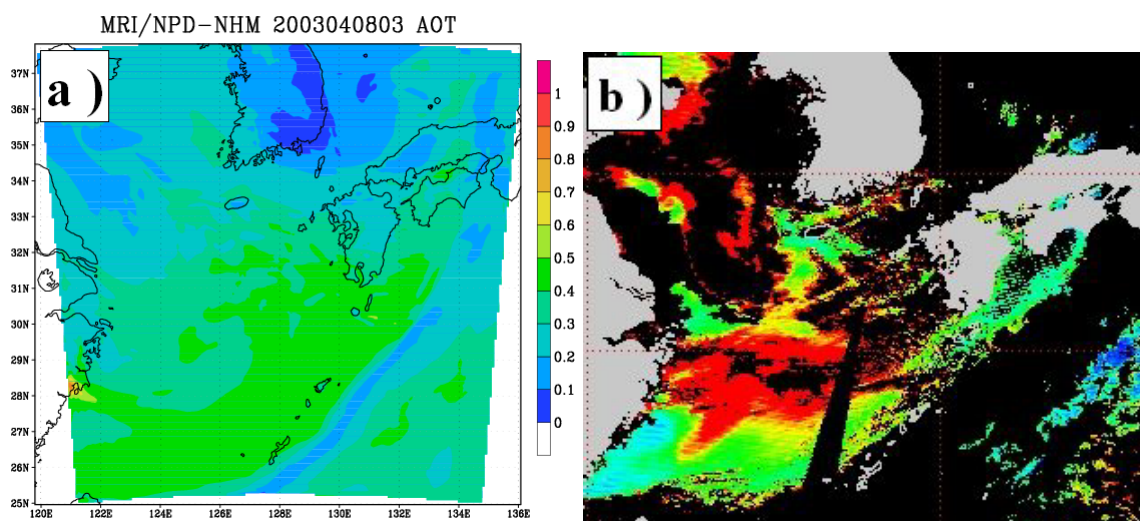


Figure 3.4 The horizontal distributions of aerosol optical thickness (a) simulated by “Aerosol and cloud bin model” and (b) produced by Terra/MODIS image at 0300 UTC 8 April 2003.

Simulated AOT values in the East China Sea were generally about 0.5, and then the similar value in the same region was confirmed in the satellite data except for in the part where high value near 1.0 was seen along the shaded region. The high value near 1.0 may be due to the error in the process of cloud screening because erroneous blue color covered with the part in the near true-color image (Fig. 3.5).

Figure 3.6 shows horizontal distributions of simulated component ratios of AOT by each aerosol to the total AOT (Fig. 3.4 (a)). Then, figure 3.7 shows the distribution of classified

aerosol type based on the satellite classification. Simulated sulfate and carbonaceous aerosols were dominant in the western part of the domain on the border of cloud row associated with the cold front. Similar tendency is confirmed in the satellite retrieval data. On the other hand, the sea salt aerosols were dominant in the eastern part of the domain in the both Figs. 3.6 (b) and 3.7. Inhomogeneity in the distribution was due to the large emission from the sea surface where strong surface wind along the cold front occurred. Dust aerosols in the satellite retrieval are slightly seen on the sea along the eastern coast of the Kyushu Region and between the Shikoku Region and Chugoku region. The simulated component ratio of AOT for dust aerosols was high in the area of prevailing westerlies in the middle layer of the troposphere. The value was especially high on the land of the Japanese Islands because the concentration of the sea salt aerosols is relatively small on the land and on a part of the sea where is located to downwind of the land, so that the region of high dust component ratio in the satellite retrieval corresponds to the region of a relatively high concentration of dust aerosols in the simulation on the downwind part of the sea near the Japanese Islands.

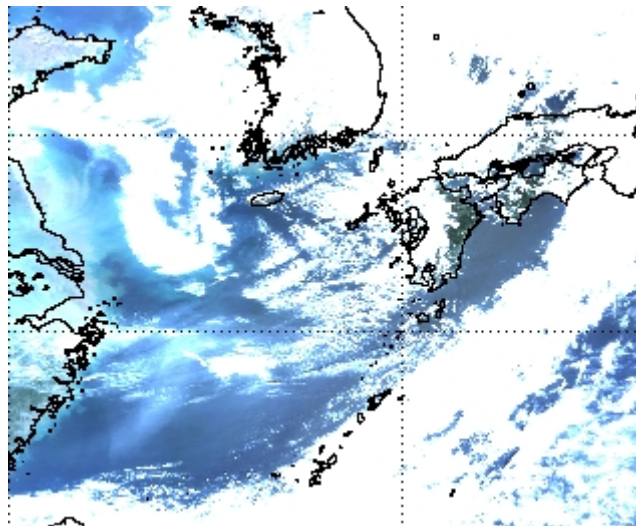


Figure 3.5 Terra/MODIS near true image on 8 April 2003.

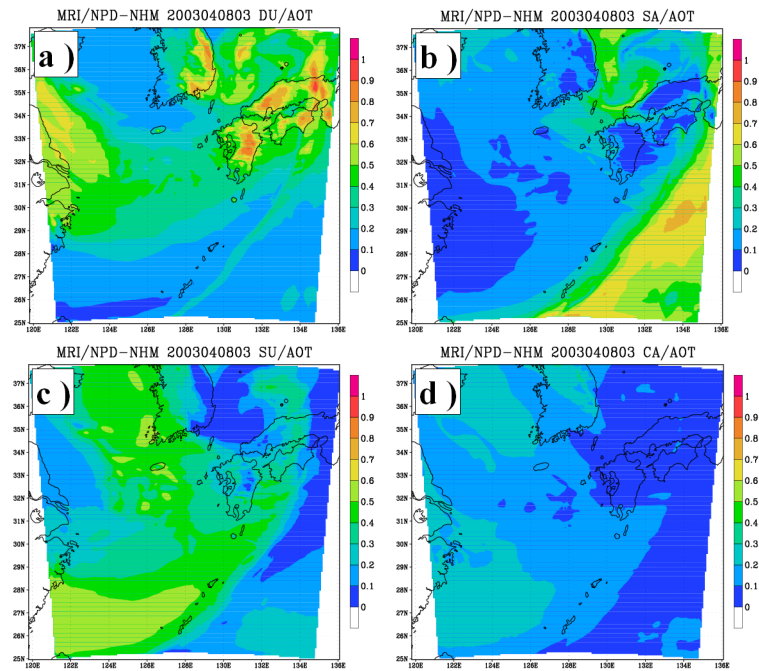


Figure 3.6 The horizontal distributions of simulated component ratios of AOT by (a) dust, (b) sea salt, (c) sulfate, and (d) carbonaceous aerosols to the total AOT at 0300 UTC 8 April 2003.

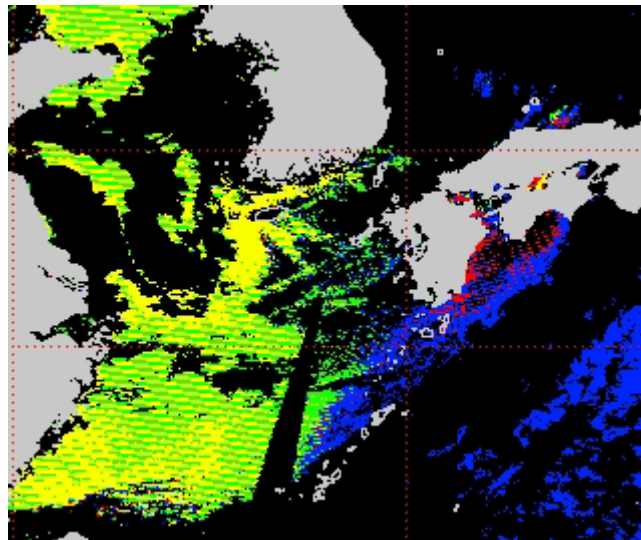


Figure 3.7 The horizontal distributions of aerosol type detected by Terra/MODIS image at 0300 UTC 8 April 2003. The aerosol types shown in panel are soil dust (red), carbonaceous (yellow), sulfate (green), and sea salt (blue) aerosols.

3.4 Conclusions

The main topic in this chapter is validating the model results through comparison of satellite-observed aerosol distributions with those simulated by ACBM nested model. The results simulated by the nested model were also compared with the results by the original SPRINTARS coupled with AGCM. Detailed spatial aerosol distributions reproduced by the regional model resembles satellite-retrieved distribution, better than that by the original SPRINTARS, because of successful calculation of accurate convective motion and scavenging process by the regional model. However, aerosols under or inside clouds, which can be activated to CCN more efficiently than in the clear sky region, are difficult to be observed by remote sensing technique, so that future airborne measurements will help better assessment of the performance of the regional model.